SUPPLEMENTARY INFORMATION

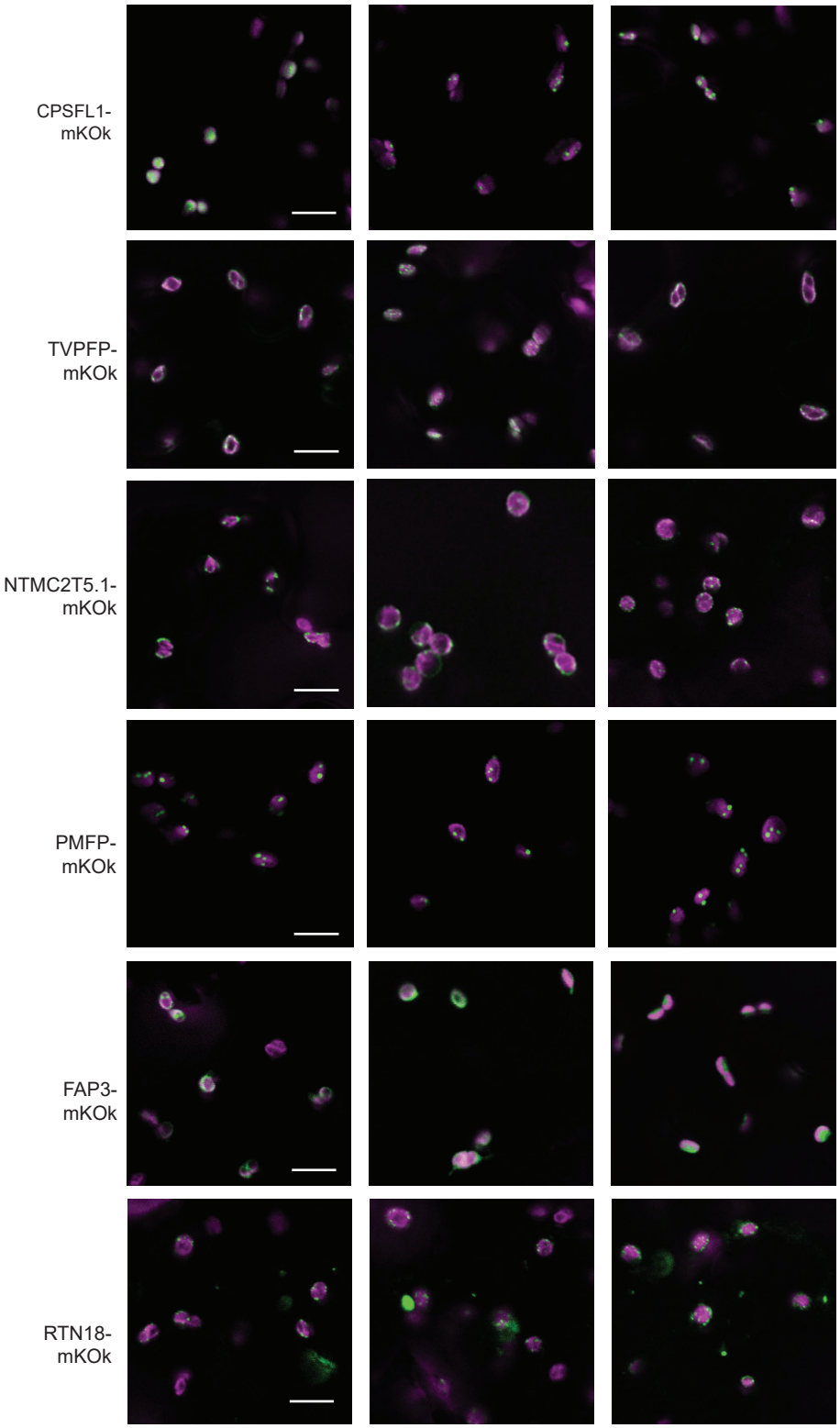

Supplementary Figure 1. Additional Confocal Images of Chloroplast Localized Candidate Proteins. Representative confocal images of mKOκ-tagged candidates expressed in *N. benthamiana.* TVPFP, NTMC2T5.1, PMFP, and RTN18 displayed punctate or reticulate fluorescence patterns suggestive of functionally specialized chloroplast regions. FAP3 exhibited a diffuse chloroplast signal. CPSFL1 showed both diffuse and punctate fluorescence, consistently overlapping with chlorophyll. Scale bar = 10 μm. Abbreviations: mKOκ, monomeric Kusabira Orange kappa; CPSFL1, CHLOROPLAST SEC14-LIKE 1; TVPFP, TVP38 FAMILY PROTEIN; NTMC2T5.1, N-TERMINAL TRANSMEMBRANE C2 DOMAIN TYPE 5.1; PMFP, PLASMA MEMBRANE FUSION PROTEIN; FAP3, FATTY ACID BINDING PROTEIN 3; RTN18, RETICULON 18.

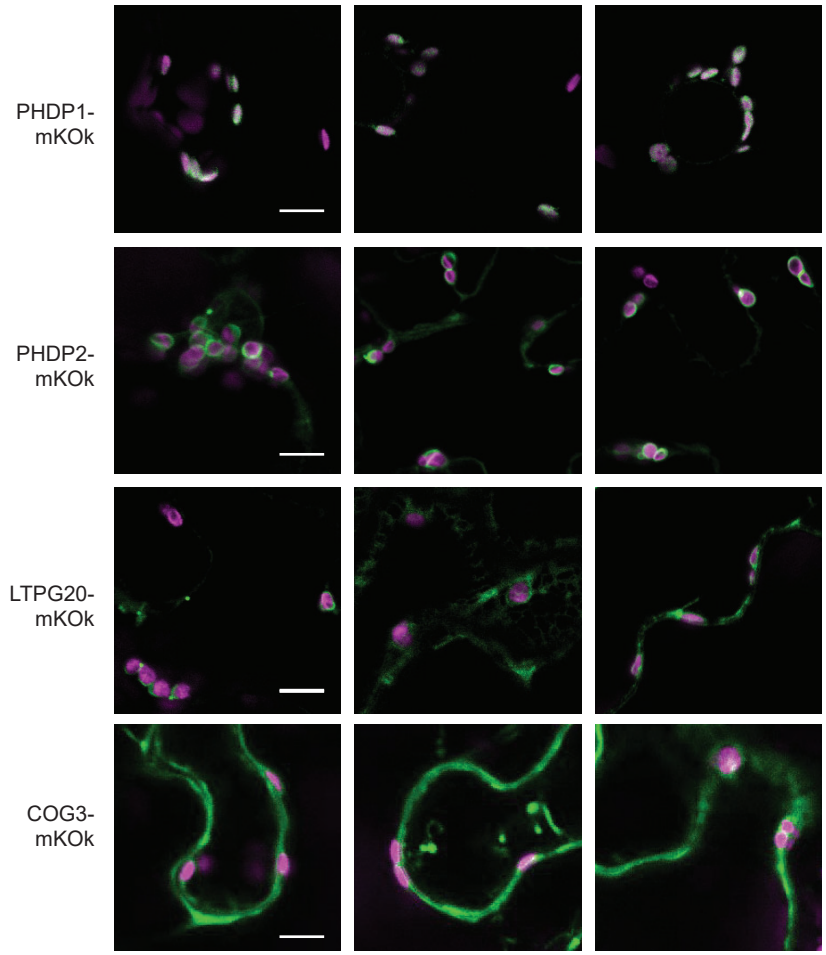

Supplementary Figure 2: Additional Confocal Images of Candidates Showing Mixed Localization. Representative confocal images of mKOκ-tagged proteins PHDP1, PHDP2, LTPG20, and COG3. PHDP1/2 showed strong but non-exclusive chloroplast association. LTPG20 and COG3 exhibited overlapping but also non-chloroplast localization. Scale bar = 10 μm. Abbreviations: mKOκ, monomeric Kusabira Orange kappa; PHDP1/2, Pleckstrin Homology Domain Protein; LTPG20, GLYCOSYLPHOSPHATIDYLINOSITOL-ANCHORED LIPID PROTEIN TRANSER 20; COG3, Conserved Oligomeric Golgi complex protein 3.

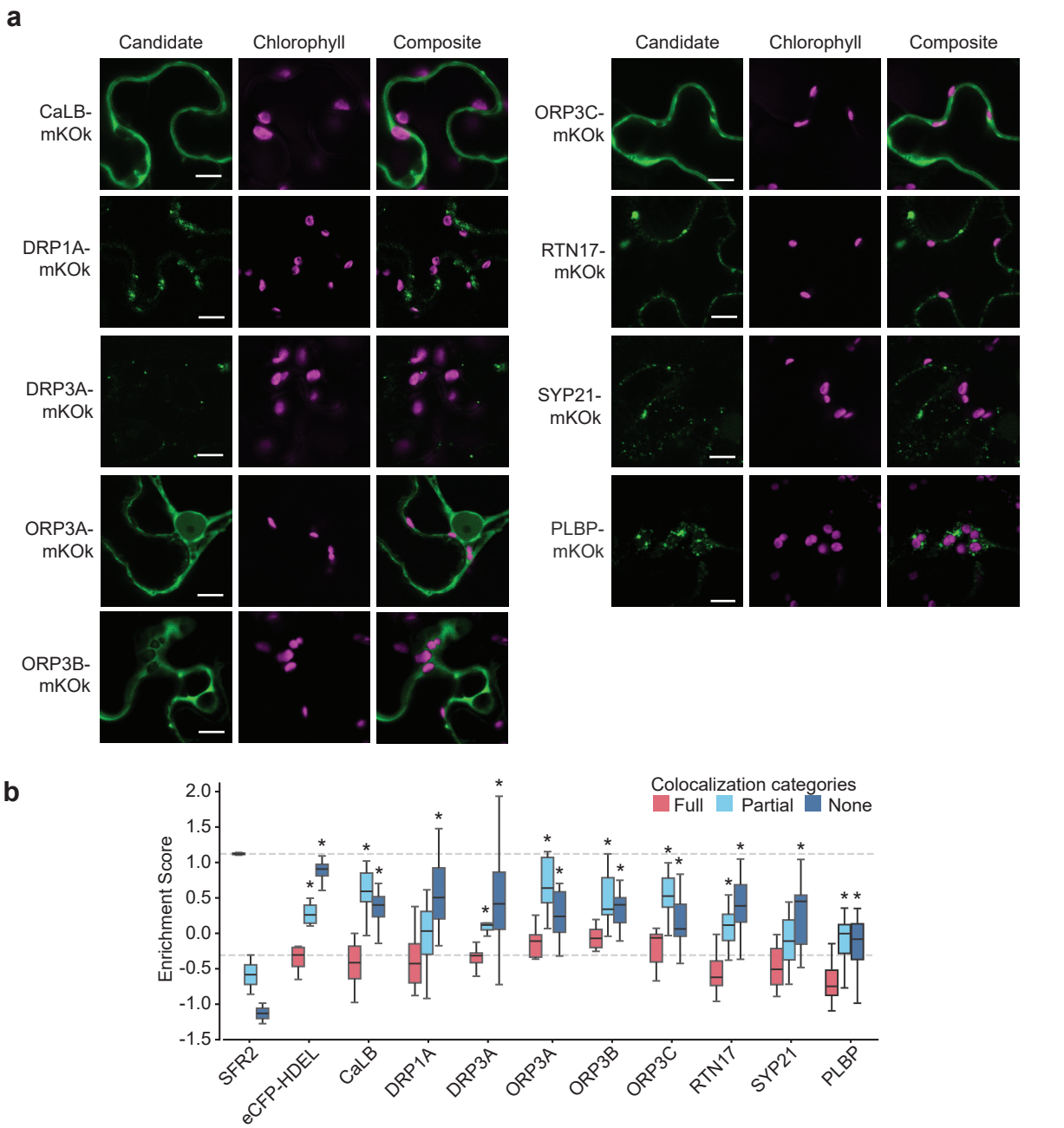

Supplementary Figure 3: Candidate Proteins Without Detectable Chloroplast Colocalization. **a** Representative confocal images of mKOκ tagged candidate proteins showing little to no overlap with chlorophyll autofluorescence. Insets = 4 × 4 µm. Scale bar = 10 µm. **b** CellProfiler-based quantification of colocalization between candidate signals and chlorophyll autofluorescence. Colocalization categories are represented as boxplots deriving from a minimum of three separate transfections, numbers of chloroplasts quantified: SFR2 *n* = 477, eCFP-HDEL *n* = 582, CaLB *n* = 777, DRP1A *n* = 860, DRP3A *n* = 1340, ORP3A *n* = 1043, ORP3B *n* = 1337, ORP3C *n* = 1558, RTN17 *n* = 1129, SYP21 *n* = 1020, PLBP *n* = 1325. Box plots show median and interquartile range (25th–75th percentiles); whiskers show min–max. Dashed lines indicate the median values for full colocalization of the positive (SFR2-eGFP) and negative (eCFP-HDEL) controls. Asterisks denote statistical significance ($p < 0.05$) by Welch's ANOVA followed by Dunnett's T3 multiple comparisons test between the full colocalization group and other categories for each protein (see Supplementary Data 2 for *p*-values). Abbreviations: mKOκ, monomeric Kusabira Orange kappa; CaLB, CALCIUM-DEPENDENT LIPID BINDING PROTEIN; DRP1A, DYNAMIN-RELATED PROTEIN 1A; DRP3A, DYNAMIN-RELATED PROTEIN 3A; ORP3A/B/C, OXYSTEROL BINDING PROTEIN 3A/B/C; RTN17, RETICULON 17; SYP21, SYNTAXIN IN PLANTS 21; PLBP, PUTATIVE LIPID BINDING PROTEIN.

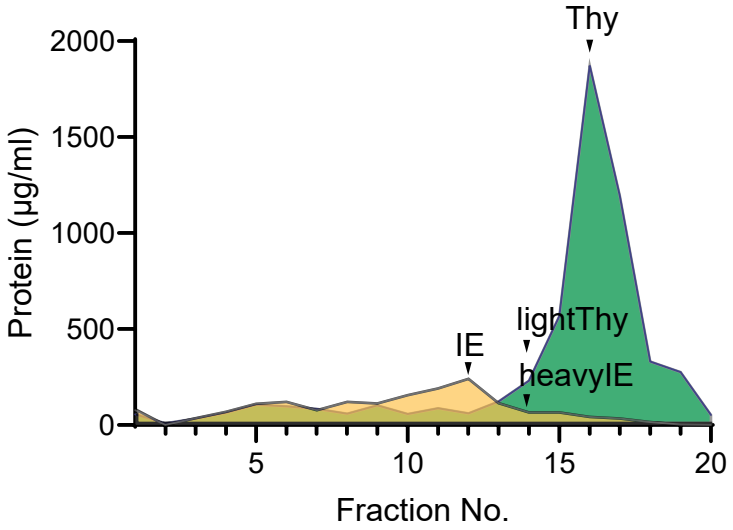

Supplementary Figure 4. Subfractionation of Chloroplast Inner Envelope and Thylakoid Membranes by Protein Content.
Chloroplast inner envelope (IE) and thylakoid membranes (Thy), isolated as described in Figure 3A and Materials and Methods, were each further separated by sedimentation through two identical continuous sucrose gradients (0.73–1.8 M). Fractions of 0.5 mL were collected and monitored for absorbance at 280 nm to estimate protein concentration (as indicated on the y-axis), they are plotted together for comparison. Aliquots (40 µl) of each fraction were analyzed by SDS-PAGE (Figure 3B), and equal amounts of protein from indicated fractions (IE – 12, heavy IE – 14; lightThy – 14, Thy 16) were precipitated and subjected to mass-spectrometry-based proteomic analysis. Subfractionation and protein measurement was repeated six times with similar results.

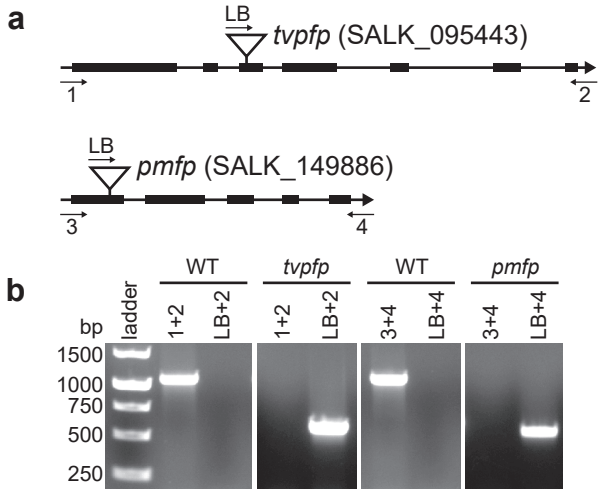

Supplementary Figure 5. PCR Verification of *tvpfp* and *pmfp* T-DNA Insertional Mutants.
a Gene models showing exon/intron structure and T-DNA insertion sites for TVPFP and PMFP. Primer binding sites are indicated. **b** PCR results for mutant genotyping. Homozygous T-DNA insertions produced expected band sizes and lacked WT-specific bands for both *tvpfp* (SALK_095443) and *pmfp* (SALK_149886). PCR was repeated five times with similar results. Abbreviations: WT, wildtype; TVPFP, TVP38 FAMILY PROTEIN; PMFP, PLASMA MEMBRANE FUSION PROTEIN.

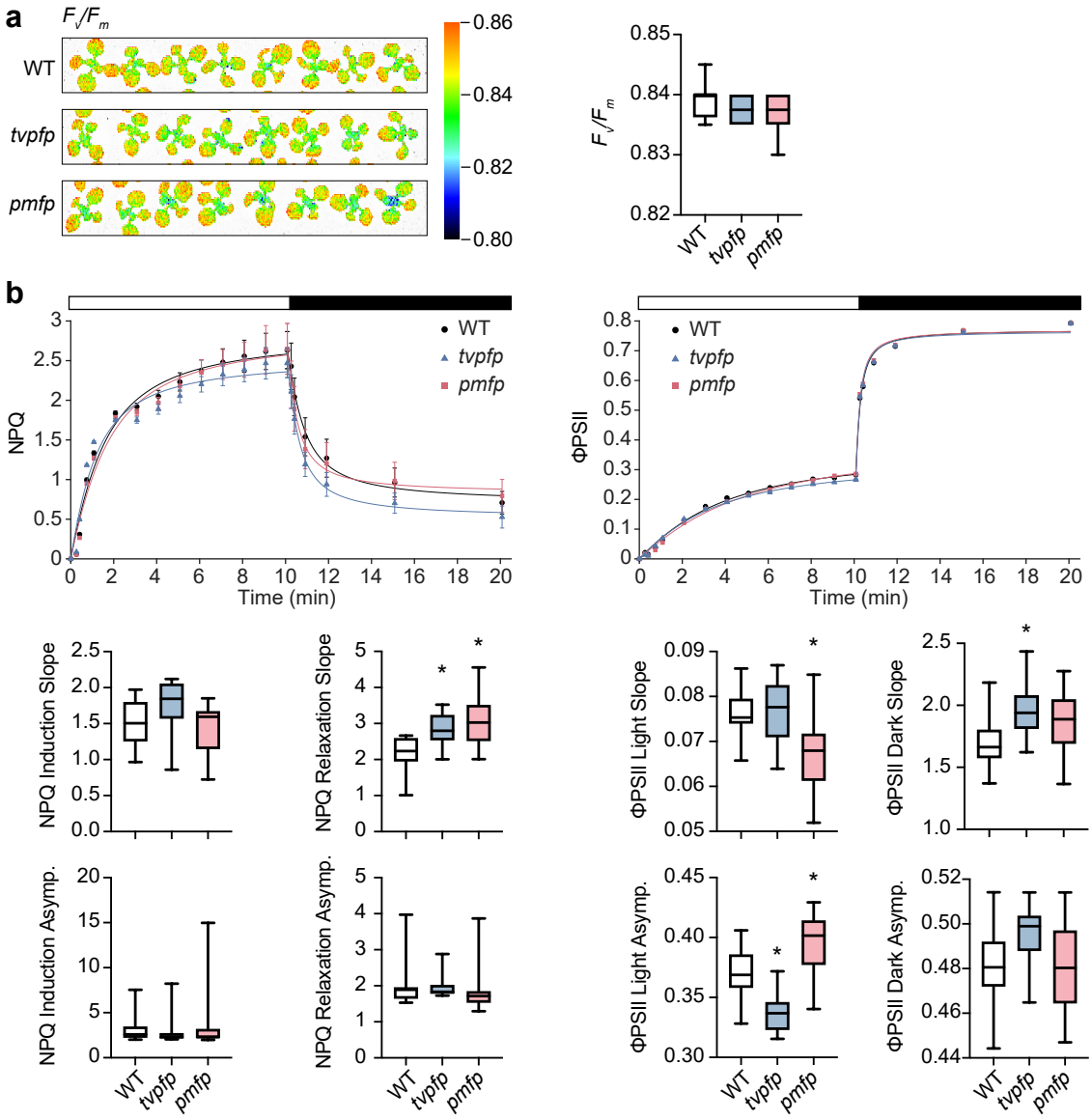

Supplementary Figure 6. Loss of TVPFP or PMFP Alters Photosystem II and Non-Photochemical Quenching Efficiency.

a Maximum quantum yield (F_v/F_m) was measured from 21-day-old rosettes after dark adaptation. F_v/F_m values from representative rosettes depicted in heatmap. **b** Nonphotochemical quenching (NPQ) and photosystem II operating efficiency (ϕPSII) kinetic parameters were measured after dark adaptation. White bar denotes light period (induction), black bar denotes dark period (relaxation/recovery). Asterisks denote statistical significance ($p \leq 0.05$) as determined by ordinary one-way ANOVA followed by Dunnett's multiple comparisons test. Box plots show median and interquartile range (25th–75th percentiles); whiskers show min–max. Biological replicates per genotype: WT (wildtype), $n = 16$; *tvpfp*, $n = 16$; *pmfp*, $n = 15$.

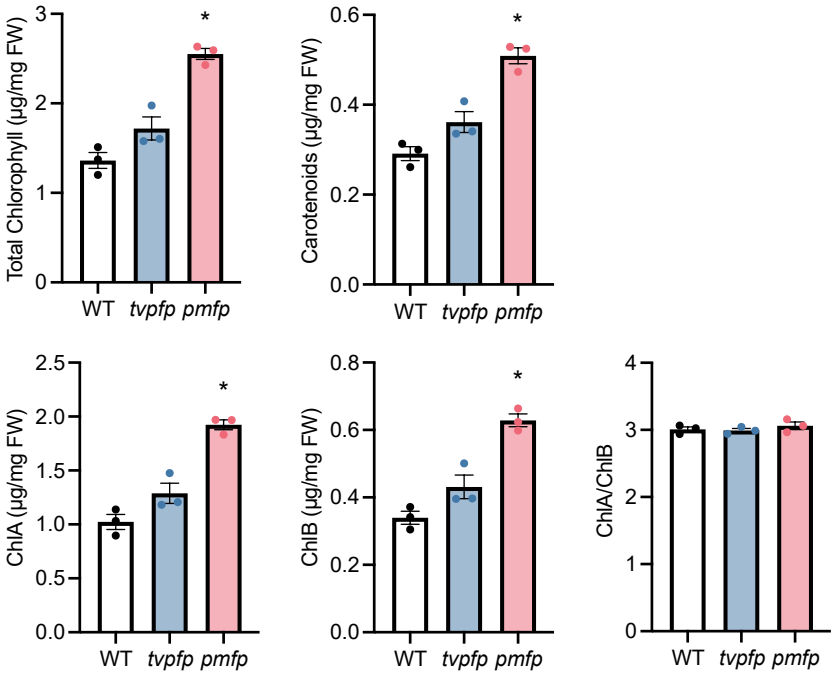

Supplementary Figure 7. Loss of PMFP Increases Chlorophyll A, B, and Carotenoids.

Pigments were extracted from five 21-day-old rosettes. Asterisks denote statistical significance ($p \leq 0.05$) as determined by ordinary one-way ANOVA followed by Dunnett's multiple comparisons test. Box plots show median and interquartile range (25th–75th percentiles); whiskers show min–max. Biological replicates $n = 3$ for all genotypes. Abbreviations: FW, fresh weight; ChlA, chlorophyll A; ChlB, chlorophyll B.

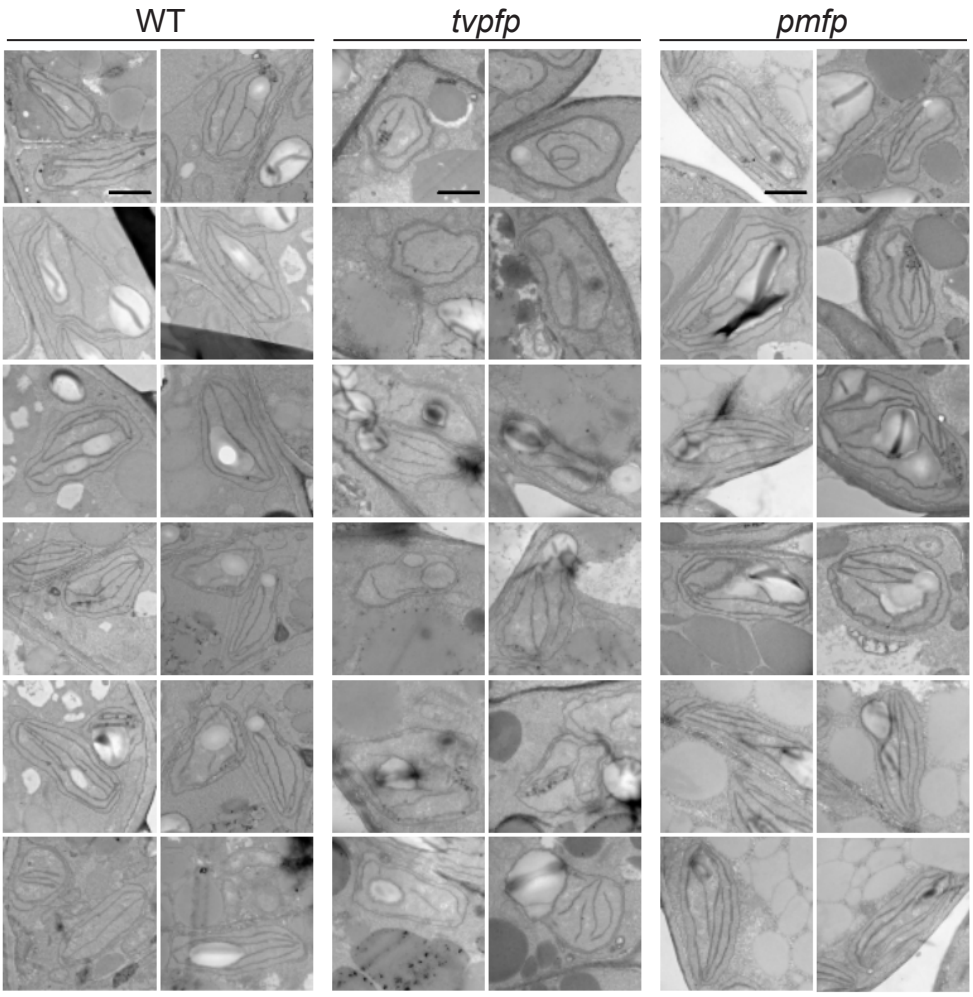

Supplementary Figure 8. Additional Transmission Electron Micrographs of *tvpfp* and *pmfp* Chloroplasts.
Transmission electron micrographs of chloroplasts from WT, *tvpfp*, and *pmfp* seedlings at 27 hours after germination in constant light. WT (wildtype) and *pmfp* plastids display typical lenticular shape and polar thylakoid-envelope proximity. *tvpfp* mutants show irregular shapes and disrupted thylakoid organization. Chloroplasts measured per genotype: WT, n = 116; *tvpfp*, n = 123; *pmfp*, n = 102; Scale bar = 1 µm.

Supplementary References

1. Hama, Y., Morishita, H. & Mizushima, N. Regulation of ER-derived membrane dynamics by the DedA domain-containing proteins VMP1 and TMEM41B. EMBO Rep. 23, 53894 (2022).

2. Huercano, C. et al. Identification of plant exclusive lipid transfer SMP proteins at membrane contact sites in Arabidopsis and Tomato. (2022) doi:10.1101/2022.12.14.520452.

3. Ngaki, M. N. et al. Evolution of the Chalcone Isomerase Fold from Fatty Acid-Binding to Stereospecific Enzyme. Nature 485, 530–533 (2012).

4. Smith, R. D. & Lupashin, V. V. Role of the conserved oligomeric Golgi (COG) complex in protein glycosylation. Sel. Pap. 14th Eur. Carbohydr. Symp. Lüb. Ger. Sept 2007 343, 2024–2031 (2008).

5. Scheffzek, K. & Welti, S. Pleckstrin homology (PH) like domains – versatile modules in protein–protein interaction platforms. FEBS Lett. 586, 2662–2673 (2012).

6. Wu, H. & Voeltz, G. K. Reticulon-3 Promotes Endosome Maturation at ER Membrane Contact Sites. Dev. Cell 56, 52-66 7 (2021).

7. Nakatsu, F. & Kawasaki, A. Functions of Oxysterol-Binding Proteins at Membrane Contact Sites and Their Control by Phosphoinositide Metabolism. Front. Cell Dev. Biol. Volume 9-2021, (2021).

8. Edqvist, J., Blomqvist, K., Nieuwland, J. & Salminen, T. A. Plant lipid transfer proteins: are we finally closing in on the roles of these enigmatic proteins? J. Lipid Res. 59, 1374–1382 (2018).

9. van de Mortel, J. E. et al. Large Expression Differences in Genes for Iron and Zinc Homeostasis, Stress Response, and Lignin Biosynthesis Distinguish Roots of Arabidopsis thaliana and the Related Metal Hyperaccumulator Thlaspi caerulescens. Plant Physiol. 142, 1127–1147 (2006).

10. Mano, S., Nakamori, C., Kondo, M., Hayashi, M. & Nishimura, M. An Arabidopsis dynamin-related protein, DRP3A, controls both peroxisomal and mitochondrial division. Plant J. 38, 487–498 (2004).

11. Sanderfoot Anton A., Kovaleva Valya, Bassham Diane C., Raikhel Natasha V., & Scheller Richard H. Interactions between Syntaxins Identify at Least Five SNARE Complexes within the Golgi/Prevacuolar System of the Arabidopsis Cell. Mol. Biol. Cell 12, 3733–3743 (2001).

12. Prinz, W. A. Bridging the gap: Membrane contact sites in signaling, metabolism, and organelle dynamics. J. Cell Biol. 205, 759–769 (2014).

13. Mi, H. et al. PANTHER version 16: A revised family classification, tree-based classification tool, enhancer regions and extensive API. Nucleic Acids Res. 49, 394–403 (2021).

14. Cho, W. & Stahelin, R. V. Membrane binding and subcellular targeting of C2 domains. Biochim. Biophys. Acta BBA - Mol. Cell Biol. Lipids 1761, 838–849 (2006).

15. Hertle, A. P. et al. A Sec14 domain protein is required for photoautotrophic growth and chloroplast vesicle formation in Arabidopsis thaliana. Proc. Natl. Acad. Sci. 117, 9101–9111 (2020).